STM JOURNALS

Journal of
Polymer & Composites

ISSN: 2321-2810 (Online)
ISSN: 2321-8525 (Print)
Volume 12, Special Issue 2, 2024
DOI (Journal): 10.37591/JoPC

http://engineeringjournals.stmjournals.in/index.php/JoPC/index

Research JoPC

Numerical Simulation and Artificial Neural Network Illustration of Phase-Change Material Integrated into Lattice Structures Printed In 3D

Deepak Kumar Yadav[1,*], Rajeev Kumar Singh[2], Arvind Kumar Gupta[3], Pushpendra Kumar Singh Rathore[4], Basant Singh Sikarwar[5]

Abstract

This work examines the phase change material (P.C.M.) deposited in various lattice formations—such as "S.C., B.C.C., and F.C.C"-at varied characteristics. The test concentrates on comprehending heat transport properties and thermal activity throughout the "melting and solidification processes". The heater's maximum temperature, P.C.M. "melting and solidification", and Nusselt number are among the essential factors examined. According to the findings, the heater's maximum temperature drops as porosity increases. Although the Nusselt values for the various lattice forms are similar, the S.C. lattice has a slightly higher Nusselt number. As porosity increases, so are the periods required for melting and solidification. Three essential parameters are predicted using an artificial neural network trained using the Bayesian Regularisation approach. The network's input parameters are set to porosity and time. When assessing the performance of P.C.M. with three lattice structures, the optimum structure of the ANN demonstrates excellent accuracy. 0.00003601 is the minimal mean square error, while 0.9998 is the most significant correlation coefficient. The trained artificial neural network (ANN) forecasts P.C.M. behaviour with 82% "S.C., B.C.C., and F.C.C". An exact match between the simulation and the ANN predictions for P.C.M. with 82% porosity lattice structures is found.

Keywords: Phase change material, Nusselt Values, lattice structures, solidification, resistance

INTRODUCTION

***Author for Correspondence**
Deepak Kumar Yadav

[1]Research Scholar Department of Mechanical Engineering, Amity University Uttar Pradesh, Noida, Uttar Pradesh India
[2]Associate Professor, Department of Mechanical Engineering, Amity University Uttar Pradesh, Noida, Uttar Pradesh India
[3]Professor, Department of Mechanical Engineering, J.C. Bose University of Science and Technology, YMCA, Faridabad, Haryana India
[4]Associate Professor, Department of Mechanical Engineering, Amity University Uttar Pradesh, Noida, Uttar Pradesh India
[5]Professor, Department of Mechanical Engineering, Amity University Uttar Pradesh, Noida, Uttar Pradesh India

Received Date: March 22, 2024
Accepted Date: May 11, 2024
Published Date: June 28, 2024

Citation: Deepak Kumar Yadav, Rajeev Kumar Singh, Arvind Kumar Gupta, Pushpendra Kumar Singh Rathore, Basant Singh Sikarwar. Numerical simulation and Artificial neural network illustration of phase-change material integrated into lattice structures printed in 3D. Journal of Polymer & Composites. 2024; 12(Special Issue 2): S175–S183p.

The progress of modern civilization has been tremendously facilitated by technological advancements that have increased the efficacy and quality of our everyday lives. In recent years, electronics have developed quickly. However, there is a constant drive for slimness, lightweight design, and miniaturization as the market for electronic products expands. Given that these devices produce more heat than they are consuming, this presents a significant problem for thermal management [1]. Numerous micro and power electronics sectors faced the difficult challenge of dissipating huge heat flux quantity, reaching roughly 300 W/cm^2, according to a 2007 research [2].

All the while making sure that the temperature didn't get over 85 °C. Modern server equipment chips now have a heat flow magnitude of up to 1 M.W./m2 [3]. Thermal problems account for

around 55% of electronic malfunctions [4]. Integrating an operational thermal management system with the electronic system is crucial for achieving optimal efficiency and dependability. P.C.M.s have significant latent heat of fusion per unit volume, among other intrinsic thermal features. It is a widely used cooling method for power electronics and is very effective [5]. P.C.M. cooling systems are more appropriate for intermittent-use electronic components than continuous-use ones because melted P.C.M. must solidify and discharge heat into the surrounding environment. P.C.M.s are intriguing, but their low heat conductivity—which leads to low melting and solidification rates—limits them. When employing P.C.M.s, thermal conductivity enhancers, or T.C.E.s, are necessary. Researchers have conducted many studies to investigate various T.C.E.s utilized in PCM-based thermal systems [6,7]. Numerous T.C.E.s, such as ("metallic fins, metallic foams, carbon foams, and so forth"), are suggested and studied [8,9]. Numerous studies have been done on metallic fins, namely plate and pin fins [10]. These fins' form [11], number [12], thickness [13], and other characteristics have all undergone extensive research and optimization. Furthermore, research has concentrated on investigating the metallic and carbon foams' porosity [14], pore density [15], and pore size [16] [17]. The development of additive manufacturing (AM) makes it feasible to produce intricate, robust, and lightweight lattice structures that are not achievable with conventional manufacturing [18]. Three types of lattice structures may be distinguished: strut-based, triply periodic minimum surface, and shell formation. Lattice structures comprise several repeating topological ordered unit cells [19]. Linking strut components at certain nodes characterizes strut-based lattice structures, including diamond, B.C.C., F.C.C., P.C., and octet-truss lattice category [20]. Lattice structures can improve the efficiency of heat "conduction and convection" because of their lightweight design and superior heat dissipation capabilities [21]. Its thermal and flow properties have been investigated and reported [22]. Several researchers used the lattice structures as T.C.E.s for the PCM-based thermal system. To improve the thermal conductivity of P.C.M., Righetti et al. [23, 24] created novel 3D metallic periodic structures using additive manufacturing. Experimental research was conducted by Piacquatio et al. [25] to evaluate the P.C.M. combined with additively built lattice structures. Four lattice configurations with identical dimensions, strut diameters, and aspect ratios but different cell topological structures were produced and put through testing. P.C.M. was implanted into multidimensional printed periodic metal foam by Zhou et al. [26], and an experimental representation of the melting process was produced. They discovered that by combining P.C.M. with periodic metal foam, the melting time might be shortened by 2.5 times. To improve the thermal conductivity of P.C.M., Hu et al. [27] created and produced a framed porous material using 3D printing. They subsequently did experimental and computational research on a heat sink that included P.C.M. with various porosities and heater powers. Using the technique of additive manufacturing, Diani et al. [30] created two periodic B.C.C. structures made of aluminium and placed three P.C.M.s with varying melting temperatures within them. The B.C.C. structures' porosity was set at 87%. To improve P.C.M.'s heat conductivity, Zhang et al. created a graded periodic cell framework that was printed using three-dimensional (3D) printing. The internal cell porosity distribution and the thickness of the exterior packing wall had an important influence on the phase change process, according to what was found in a three-dimensional numerical simulation model confirmed by experimental data. Numerical research on the performance enhancement of P.C.M. implanted in metal periodic structures was conducted by Zhao et al. The influence of material qualities, cell elevation thickness of interaction gap, and cell size were examined and discussed [28]. To determine the impact of porosity and grading of "triply periodic minimum surface" structures on P.C.M.'s thermal performance, Qureshi et al. conducted numerical simulations. Four TPMS configurations with various permeability were taken into account. After setting the overall porosity at 75%, the scientists looked at the impacts of a uniform, positive, and negative porosity gradient. Artificial neural networks (ANNs) have been used more often in recent years to analyze and predict phase and heat transfer shifts in P.C.M.s. The process of emulating biological neural networks results in ANNs. Because they have so many neurons, artificial neural networks (ANNs) are very good at handling non-linear problems, demonstrating error resistance, and easily handling noisy or missing data. These networks can develop from training data, and after they have finished training, they solve problems incredibly well. Consequently, the trained model may be applied to predict desired parameters in analogous situations. ANN was used by Urresti et al. [29] to investigate and assess the thermal behaviour of P.C.M.s integrated into building envelopes using experimental data. Using experimental data, Motahar used

ANN to estimate percentage in an enclosure. To forecast the temperature, liquid fraction, and Nusselt number for a P.C.M. with a metallic foam system dependent on time and porosity, Duan et al. used artificial neural networks (ANN) with experimental data. Despite their growing popularity in this domain, there is currently little published research on the use of ANNs in P.C.M. modelling and prediction for heat transfer. This research pertains to the prediction and optimization of P.C.M. performance with integrated lattice structures. In the present study, we examine the possibility of using artificially generated neural networks to forecast the "dynamic melting and solidification process" of P.C.M. embedded with three different kinds of lattice structures: S.C., B.C.C., and F.C.C. The numerical simulations are run under six porosity levels of three lattice configurations, ranging from 70% to 95%, and are confirmed by experimental proof. Measurements, including the heat wall's maximum temperature, the time it takes for "melting and solidifying", and the Nusselt number, are compared and evaluated at different porosity levels. The ANN analysis that follows uses the data produced by the numerical simulation. To forecast the temperature of the heat wall, the melting and solidification of P.C.M., and the Nusselt number, an M.L.P. "multilayer perceptron" "feed-forward neural network" constructed depend on the Bayesian Normalisation (B.R.) method has been built. When forecasting the heat transfer pattern, the created ANN has an ideal structure and outstanding precision.

Geometries And Simulation Models

Several crystalline structures—"S.C., B.C.C., and F.C.C."—are employed as T.C.E.s in the investigation, as Fig. 1 illustrates (Table 1). The metal ligaments in S.C.'s structure have been organized in a periodic cubic cell configuration, with connections at right angles. Homogeneous struts with equal cross-sections are a defining feature of the crystal molecules' body frameworks known as the B.C.C. and F.C.C. structures. The positioning of atoms in the unit cell, which built distinct coordination arms and packing densities, is the primary distinction between the F.C.C. and B.C.C. lattice structures. The thermal performance of these three lattice structures—whose porosities range from 70% to 95%—is examined and contrasted after merging with P.C.M. Table 1 lists the measurements correlating to the varying porosities. There are four × four x four lattice structures in all. With a 5 kW/m2 heat flux, the heat source in that configuration is positioned at the cube's bottom wall. After 3000s, the heat source is switched off to give the P.C.M. time to harden. A "natural convection boundary" situation with a convective coefficient of 8W/m^2 K is applied to the remaining cube's walls. In the present research, RT50 is employed. Its latent heat is 160 kJ/kg, and its defrost range is 45–51 ◦C. RT50 has a specific heat of 2000J/kgK, thermal conductivity of 0.2W/mK, and 880 kg/m3 density.

Border conditions and controlling equations the governing formulas Numerical studies in three dimensions are carried out to simulate P.C.M. melting and the process of solidification. The following presumptions are made to make the simulation more straightforward: The aluminium P.C.M. case is consistent and isotropic; the aluminium's thermophysical characteristics are stable and temperature-insensitive. The controlling formulas for phase transition and heat transmission in P.C.M. embedded in lattice structures are solved using ANSYS 2020R2. The phase transition between P.C.M.'s fluid and solid states is defined by activating the solidification and melting model mechanism. Instead of explicitly monitoring the liquid-solid interface in this model, an enthalpy-porosity formulation views the liquid-solid mushy zone as a porous zone whose porosity is equal to the liquid percentage. Each iteration calculates the liquid fraction, the percentage of liquid form in a cell volume. This parameter's value ranges from 0 to 1 in the gooey zone. The following are the equations that dictate for the P.C.M. heat sink:

Continuity equation:

$$\frac{\partial \rho}{\partial t} + \frac{\partial u}{\partial x} + \frac{\partial v}{\partial y} = 0 \quad (1)$$

Momentum equation:

$$\frac{\partial(\rho u)}{\partial t} + \frac{\partial(\rho u u)}{\partial x} + \frac{\partial(\rho u v)}{\partial y} = -\frac{\partial P}{\partial x} + \mu\left(\frac{\partial^2 u}{\partial x^2} + \frac{\partial^2 u}{\partial y^2}\right) + Sx \text{ in x- dir} \quad (2)$$

$$\frac{\partial(\rho v)}{\partial t}+\frac{\partial(\rho uv)}{\partial x}+\frac{\partial(\rho vv)}{\partial y}=-\frac{\partial P}{\partial y}+\mu\left(\frac{\partial^2 v}{\partial x^2}+\frac{\partial^2 v}{\partial y^2}\right)+Sy-\rho\text{gin y- dir} \quad (3)$$

Energy equation:

$$\frac{\partial(\rho H)}{\partial t}+\frac{\partial(\rho uH)}{\partial x}+\frac{\partial(\rho vH)}{\partial y}=+k\left(\frac{\partial^2 T}{\partial x^2}+\frac{\partial^2 T}{\partial y^2}\right) \quad (4)$$

The variables in Eqs. (1)–(4) are time (t), velocity (u) and velocity (v) in the x & y directions accordingly. P stands for pressure, μ for P.C.M.'s dynamic viscosity, and g for the acceleration of gravity. ρ denotes the P.C.M. density. The Boussinesq method accounts for density change linked to buoyancy forces and enables natural convection realisation during P.C.M. defrost. The momentum sink terms, Sx and Sy, in Eqs. (2) and (3) are the result of the mushy zone's reducing porosity and are defined as below:

$$S_x=C_{mush}\frac{(1-\beta)^2}{(\beta^3+\epsilon)}u \quad (5)$$

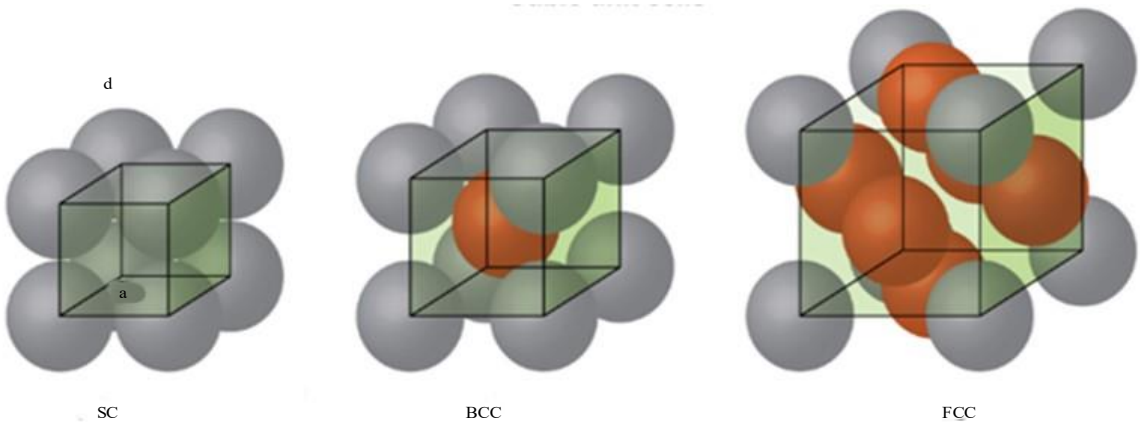

Figure 1. Shows heat sinks geometries.

Table 1. heat sinks geometries in mm

"Lattice structures"	"Porosity"	"Length"	"Diameter"	"Total body volume of unit structures mm^3"
(SC)	95	10	0.6	50
(B.C.C.)			1	
(F.C.C.)			1.1	
(SC)	85	10	1.2	150
(B.C.C.)			1.8	
(F.C.C.)			2.0	
(SC)	75	10	1.6	250
(B.C.C.)			2.4	
(F.C.C.)			2.7	
(SC)	65	10	1.8	350
(B.C.C.)			2.1	
(F.C.C.)			2.4	
(SC)	55	10	1.9	450
(B.C.C.)			2.4	
(F.C.C.)			2.8	

Sy = C mush (1 − β) 2 (β3 + ϵ) v (7) where β is the liquid percentage of P.C.M. and is specified as follows, ϵ is a tiny value of 0.001 to prevent zero numerators, and C mush is the mushy zone constant, which is set at 105 in the present research.

T – T solidus /T liquids – T solidus, if T solidus < T < T liquids (8)

The enthalpy of P.C.M., denoted as H in Eq. (4), is the product of the sensible enthalpy, h, and the latent heat, ΔH: H = h + ΔH (9) Cp (T − Tinitial) + h initial = h (10) ΔH = βL (11) is where L is the latent heat of fusion of P.C.M., Cp is the specific heat of P.C.M., and the starting enthalpy and temperature of P.C.M. are initial and initial, respectively. The PRESTO! method applies for pressure discretization in solving these equations, while the PISO method is employed to couple the two variables. The P.C.M.'s starting temperature is 293K (20 ◦C). The simulation uses conditions for laminar flow. There is no slip surface on the wall.

Model confirmation, mesh, and time scale independent verification

The present examination's simulation results have been verified using a comparison with the experimental data reported in Reference [28]. The comparison between the temperature between the experimental and numerical data using the identical P.C.M. (Rubitherm RT62HC), boundary conditions, and geometric model as mentioned in Reference [28]. Notably, the simulation results show a strong correlation with the experimental data, indicating the validity of the simulation approach. The simulation model's accuracy and precision are further confirmed by the finding that the most significant proportional variation between the numerical temperature and the equivalent observed value is just 2.5%. The validation test demonstrates the simulation results' reliability and validity and provides evidence supporting the study's conclusions. A tetrahedral mesh is used to discretize the numerical models, and a trio of cell mesh sizes—65,000, 95,000, and 162,000—are investigated. The results of the simulations with the three different mesh numbers show a perfect consistency. Because it yields correct results with a reduced effort, a mesh number of 65,000 is chosen to maximize computational efficiency. An examination with the simulation results obtained via 0.50s, 0.20s, and 0.10s time increased. There is much resemblance between the outcomes generated by the three distinct time stages. This suggests that the time step selection does not significantly impact the accuracy of the results of simulations. Consequently, 0.5s is chosen as the time step for this investigation as it requires fewer computing resources.

Artificial Neural Network

The design and action of the natural neural networks seen in the human brain served as the model's inspiration for the artificial neural network, or ANN. It is a machine-learning algorithm comprising linked nodes arranged in layers—also called artificial neurons. After receiving input data, the neurons apply an actuation task to create nonlinearity, conduct a weighted sum of the inputs, and then produce an output. The weights attached to relationships between neurons control how strong the signal is sent from one neuron to the next. By analyzing patterns and correlations in the training data, artificial neural networks (ANNs) may adjust their internal weights by learning from the data. The network modifies the weights to reduce prediction errors throughout training by comparing its predictions with the correct outputs. It is an effective technique for managing intricate and non-linear data interactions. Because there are significant differences between the data points, the data should be normalized before beginning ANN network training to improve network performance. Equation (12) is used in the standardization method to scale the data to a range of 0–1.

$$xi,norm = xi - xmin / xmax - xmin \quad (12)$$

here, xmax and xmin are the highest and lowest values and xi; norm is the acceptable value. To evaluate the efficacy and precision of the ANN network's predictions, the mean square deviation (M.S.E.) and Pearson's correlation coefficient (R) are defined as follows:

$$\text{MSM} = \frac{1}{\text{m}} \sum_{j=1}^{m} \left(y_j^{SIM} - y_j^{ANN} \right)$$

$$R = \frac{\frac{1}{\text{m}} \sum_{j=1}^{m} \left(y_j^{SIM} - y^{SIM} \right) \left(y_j^{ANN} - y^{ANN} \right)}{\sqrt{\sum_{j=1}^{m} \left(y_j^{SIM} - y^{SIM} \right)^2 \sum_{j=1}^{m} (y_j^{ANN} - y^{ANM})^2}}$$

Where m is the number of the simulation data, ySIM j is the j-th simulation result, and yANN j is the calculated result of the j-th data by using.

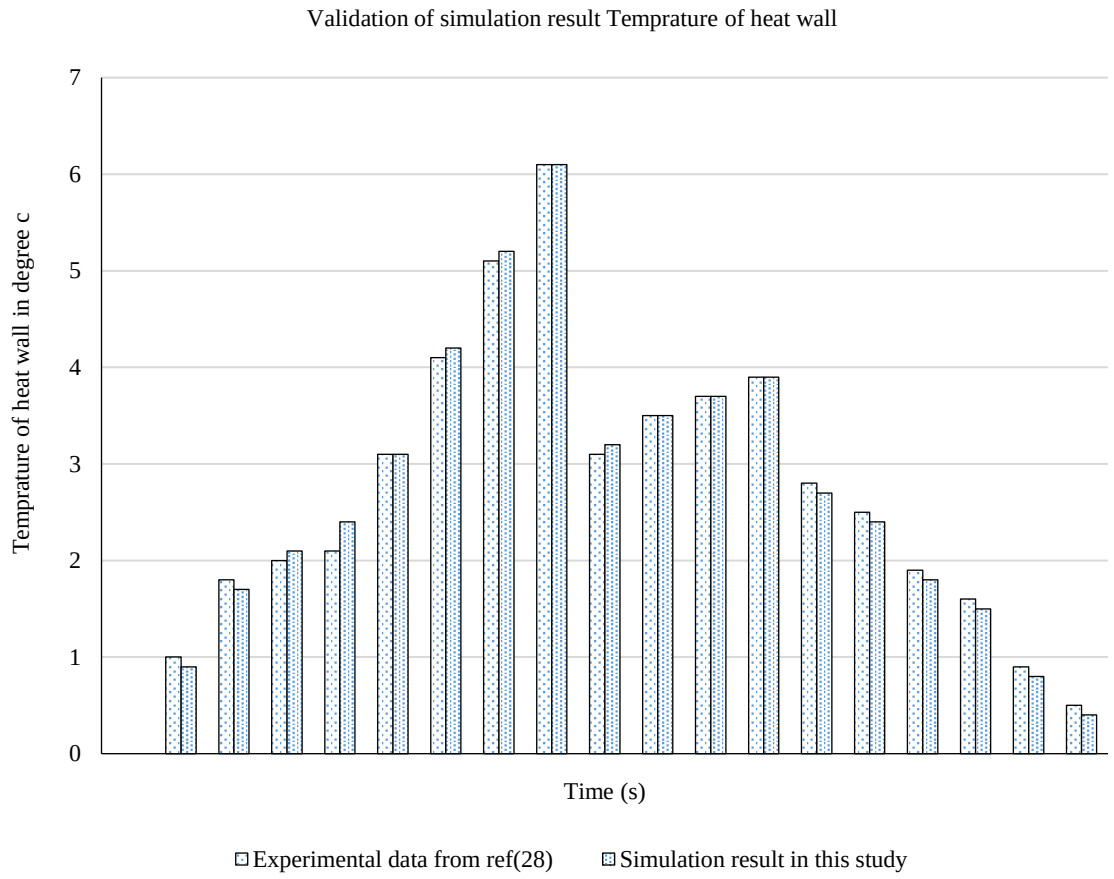

Figure 2. This figure shows the validation of stimulation result temperature of heat wall.

A standard deviation of ANN and y is the value. Three fundamental layers comprise a neural network of neurons (ANN): an i/p layer, an unseen layer, and an o/p layer. Two nodes make up the i/p layer of the network: normalized time and adjusted porosity of lattice structures. Three nodes comprise the output layer: the Nu number, the P.C.M. liquid percentage, and the temperature of the heat wall. Using information from numerical modelling, the Back-propagation approach is used to train the artificial neural network. The Bayesian Regularisation (B.R.) technique is used for regression applications. Upon comparing the learning performance of Scaled Conjugate Gradient (S.C.G.) ANN, Levenberg-Marquardt (L.M.) ANN and BR ANN, it is clear that BR ANN is more capable of learning than LM ANN and SCG ANN. Three groups are created from the numerical simulation's data. For three different kinds of lattice architectures, three different networks are trained. The degree of disorder, based on the number of nodes in the hidden layer, significantly impacts ANN accuracy diagram -2. The hidden-layer node count is changed from five to fifty. When the number of hidden-layer nodes is set to 25, the network model's mean square error (M.S.E.) decreases when the BR ANN training results are analyzed after each modification. In addition, every ANN regression produces a correlation coefficient (R) greater than 0.99, suggesting a solid agreement among the simulation outcomes and the ANN outputs.

RESULTS AND DISCUSSIONS

Findings of the RT50 embedded lattice structure modelling The simulation outcomes of RT50 joined with various lattice structures “S.C., B.C.C., and F.C.C." across varying porosity under a 5 kW/m2 heat flux, in particular, show the heat wall's temperature. At first, the melting process starts when the RT50

temperature hits 45 °C, and the wall temperature climbs quickly. At this stage, the P.C.M. melting process absorbs a considerable quantity of heat, which causes the wall temperature to rise more slowly. Complete melting occurs when the RT50 temperature reaches 51 ◦C, preventing the P.C.M. from absorbing more heat. There is a rapid increase in the wall's temp. The heat supply is cut off when the wall temperature reaches its maximum value at 3000s. Natural air convection cooling causes the wall temperature to drop progressively. The solidification process begins when the RT50 temperature falls below its solidification point, releasing heat. For this reason, the wall temperature gradually drops throughout the solidification phase. After the P.C.M. solidifies completely, the wall temperature drops very quickly. The heat wall reaches its maximum temperature at 3000s when the lattice structure porosity is 70%. Porosity and the heat wall's maximum temperature are shown to be inversely related. The heat wall's maximum temperature falls as porosity progressively rises. This link is explained by the fact that a lower porosity causes a smaller quantity of RT50, which raises the maximum temperature. The findings suggest that RT50 starts to melt in the 1000s and finishes melting in the 2500s. When the porosity is adjusted to 95% in all three lattice scenarios, RT50 shows an earlier melting onset and a longer melting duration than other porosity levels. RT50 has the fastest melting rate, notably at a lattice porosity of 70%. The RT50 melting speed rose as the lattice porosity progressively decreased. This tendency may be explained by the positive impact of a higher lattice volume, which is correlated with reduced porosity. Faster melting rates are achieved by the P.C.M.'s improved heat conductivity, which is facilitated by this bigger volume. Approximately 4000s marks the start of RT50's solidification, while 8000s marks its completion. RT50 shows a faster commencement of solidification and a longer solidification process duration when the porosity is set at 95% as opposed to other porosity levels. The solidification speed of RT50 increased with a steady reduction in lattice porosity. The Nusselt number of the RT50 when combined with the S.C., B.C.C., and F.C.C. lattice structures, respectively. Because the convective heat transmission methods shift during the P.C.M. melting and solidification process, the Nusselt number also tends to change. The liquid fraction contours when RT50 is implanted with S.C., B.C.C., and F.C.C., respectively. First, there is a rise in the Nusselt number when the P.C.M. next to the heat wall starts to melt. This is frequently explained by the increased convective heat transfer brought about by the fluid phase's presence close to the walls, which encourages mixing and convection currents. The RT50 melting process begins at the bottom and moves towards the top as thermal energy is transferred from the bottom heat wall to the side wall. In addition, heat moves through lattice structures from the side wall into the interior region simultaneously, affecting the P.C.M's phase transition. The Nusselt number reaches its maximum when the RT50 close to every wall has melted entirely. Since convective heat transport has already begun in such areas, the Nusselt number stays mostly unchanged as the melting process moves towards the core region. A decrease in convective heat transmission results from the liquid P.C.M.'s slowing motion while the RT50 keeps melting. The Nusselt number decreases as the melting process progresses due to this decrease in heat transmission efficiency. Following total melting, the liquid P.C.M. gradually comes to a halt, causing the Nusselt number to fall steadily. The heat power is turned off at around 3000 s, which causes the Nusselt number to abruptly fall below 0. This indicates that natural air convection transfers heat from the system to the surrounding area. The RT50 then starts to solidify when its temperature hits its solidification point. In the early solidification phases, there is a brief increase in the Nusselt number's absolute value. The solidification process is shown to start close to the wall and is driven by natural convection from the outside air. The Nusselt value remains constant as the P.C.M. solidifies closer to the interior. Nonetheless, the Nusselt number usually drops as the P.C.M. completely hardens and the solidification process proceeds. There may be a tiny additional fall in the Nusselt value if the P.C.M. solidifies entirely. This is explained by the convective heat transfer mechanism being impacted by the system's surroundings' continuously decreasing temperature differential.

CONCLUSIONS

In brief, this study's simulation results offer a remarkable understanding of the qualities of P.C.M. (RT50) when combined with diverse lattice structures (such as S.C., B.C.C., and F.C.C.) with pores varying from 70-90 per cent. The fixed heat flow of 5 kW/m^2 is maintained for 3000s before shutting

off. The experimental data from the reference has been used to validate the simulation. Because of the nonlinearity of the melting process, an artificial neural network (ANN) model is created to forecast the critical parameters of P.C.M. behaviours. Important conclusions consist of:

1. The porosity of the heat wall and its maximum temperature are inversely correlated. The maximum temperature falls as the porosity rises. Furthermore, the most excellent temperatures of the heating layer for P.C.M. implanted with all three lattice configurations are pretty similar when the lattice pores are less than 80%. On the other hand, the P.C.M. with S.C. lattice has the lowest wall temperature when the porosity surpasses 80%, whilst the P.C.M. with B.C.C. and F.C.C. lattices show equal temperatures.
2. Compared to other pore levels, P.C.M. shows a faster melting commencement and longer melting duration when the lattice porosity is 95%. Furthermore, a larger lattice volume has the beneficial consequence of increasing the P.C.M.'s heat conductivity, which causes a lower lattice porosity to result in quicker melting rates.
3. P.C.M. with the B.C.C. lattice has a slightly longer melting time than the other scenarios when the lattice porosity is less than 80%. In contrast, P.C.M. with the S.C. lattice has a somewhat longer melting time when the porosity surpasses 80%. The solidification time rises with increasing lattice porosity, much like the melting time. Compared to the other scenarios, the solidification period of the F.C.C. lattice structure is somewhat more extended.

REFERENCES

1. C. Lu *et al.* Econometrics of the environmental Kuznets curve: testing advancement to carbon intensity-oriented sustainability for eight economic zones in China, J. Clean. Prod. (2021)
2. M. Chen *et al.*Carbon Kuznets curve in China's building operations: retrospective and prospective trajectories Sci. Total Environ. (2022)
3. C. Arumugam *et al.* Air-conditioning cost saving and CO2 emission reduction perspective of buildings designed with P.C.M. integrated blocks and roofs Sustain. Energy Technol. Assessments (2021)
4. Q. Al-Yasiri *et al.* Incorporation of phase change materials into building envelope for thermal comfort and energy saving: a comprehensive analysis J. Build. Eng. (2021)
5. F. Hassan *et al.*Recent advancements in latent heat phase change materials and their applications for thermal energy storage and buildings: a state of the art review Sustain. Energy Technol. Assessments (2022)
6. R.A. Lawag *et al.* Phase change materials for thermal management and energy storage: a review J. Energy Storage (2022)
7. Q. Xiong *et al.* Application of phase change material in improving trombe wall efficiency: an up-to-date and comprehensive overview Energy Build. (2022)
8. X. Wang *et al.* A critical review on phase change materials (P.C.M.) for sustainable and energy-efficient building: design, characteristic, performance and application Energy Build. (2022)
9. P.K.S. Rathore *et al.* Enhanced thermophysical properties of organic P.C.M. through shape stabilization for thermal energy storage in buildings: a state of the art review Energy Build. (2021)
10. B. Eanest Jebasingh *et al.* A comprehensive review on latent heat and thermal conductivity of nanoparticle dispersed phase change material for low-temperature applications Energy Storage Mater. (2020)
11. I. Shamseddine *et al.* Supercooling of phase change materials: a review Renew. Sustain. Energy Rev. (2022)
12. C. Li *et al.* Experimental thermal performance of wallboard with hybrid microencapsulated phase change materials for building application J. Build. Eng. (2020)
13. C. Li *et al.* Experimental investigation of thermal performance of microencapsulated PCM-contained wallboard by two measurement modes Energy Build. (2019)
14. S. Ben Romdhane *et al.* A review on thermal energy storage using phase change materials in passive building applications J. Build. Eng. (2020)

15. K. Faraj *et al.* A review on phase change materials for thermal energy storage in buildings: heating and hybrid applications J. Energy Storage (2021)
16. B.V.S. Dinesh, A. Bhattacharya, Comparison of energy absorption characteristics of PCM-metal foam systems with different pore size distributions, J. Energy Storage 28 (2020), 101190.
17. X. Liu, F. Yang, M. Li, C. Sun, Y. Wu, Development of cost-effective PCM-carbon foam composites for thermal energy storage, Energy Rep. 8 (2022) 1696–1703.
18. C. Pan, Y. Han, J. Lu, Design and optimization of lattice structures: a review, Appl. Sci. 10 (2020) 6374.
19. T. Maconachie, M. Leary, B. Lozanovski, X. Zhang, M. Qian, O. Faruque, M. Brandt, S.L.M. lattice structures: properties, performance, applications and challenges, Mater. Des. 183 (2019), 108137.
20. M.E. Korkmaz, M.K. Gupta, G. Robak, K. Moj, G.M. Krolczyk, M. Funtoglu, Development of lattice structure with selective laser melting process: state of the art on properties, future trends and challenges, J. Manuf. Process. 81 (2022) 1040–1063.
21. U. Sajjad, T. Rehman, M. Ali, C.W. Park, W.M. Yan, Manufacturing and potential applications of lattice structures in thermal systems: a comprehensive review of recent advances, Int. J. Heat Mass Trans. 198 (2022), 123352.
22. S. Sarabhai, N. Letov, M. Kibsey, F. Sanchez, Y.F. Zhao, Understanding the flow and thermal characteristics of non-stochastic strut-based and surface-based lattice structures, Mater. Des. 227 (2023), 111787.
23. G. Righetti, L. Doretti, C. Zilio, G.A. Longo, S. Mancin, Experimental investigation of phase change of medium/high-temperature paraffin wax embedded in a 3D periodic structure, Int. J. Thermo fluids. 5–6 (2020), 100035.
24. G. Righetti, G. Savio, R. Meneghello, L. Doretti, S. Mancin, Experimental study of phase change material (P.C.M.) embedded in 3D periodic structures realized via additive manufacturing, Int. J. Therm. Sci. 153 (2020), 106376.
25. S. Piacquadio, M. Schirp-Schoenen, M. Mameli, S. Filippeschi, K.U. Schroder, Experimental analysis of a phase change material's thermal energy storage potential embedded in additively manufactured lattice structures, Appl. Therm. Eng. 216 (2022), 119091.
26. Z. Zhou, Z. Hu, D. Wang, H. Wu, Visualized-experimental investigation on the melting performance of P.C.M. in 3D printed metal foam, Therm. Sci. Eng. Prog. 31 (2022), 101298.
27. X. Hu, X. Gong, Experimental and numerical investigation on thermal performance enhancement of phase change material embedding porous metal structure with cubic cell, Appl. Therm. Eng. 175 (2020), 115337.
28. X. Hu, X. Gong, Experimental study on the thermal response of PCM-based heat sink using structured porous material fabricated by 3D printing, Case Stud. Therm. Eng. 24 (2021), 1000844.
29. X. Hu, X. Gong, Pore-scale numerical simulation of the thermal performance for phase change material embedded in metal foam with cubic periodic cell structure, Appl. Therm. Eng. 151 (2019) 231–239.
30. A. Diani, C. Nonino, L. Rossetto, Melting of phase change materials inside periodic cellular structures fabricated by additive manufacturing: experimental results and numerical simulations, Appl. Therm. Eng. 215 (2022), 118969

